INSTITUTE OF PHYSICS PUBLISHING MEASUREMENT SCIENCE AND TECHNOLOGY

Meas. Sci. Technol. **15** (2004) 254–266 PII: S0957-0233(04)66559-3

Quantifying dielectrophoretic collections of sub-micron particles on microelectrodes

D J Bakewell and H Morgan[1]

Department of Electronics and Electrical Engineering, University of Glasgow, Glasgow G12 8LT, UK

E-mail: d.bakewell@beatson.gla.ac.uk and hm@ecs.soton.ac.uk

Received 25 July 2003, in final form 20 October 2003, accepted for publication 24 October 2003
Published 28 November 2003
Online at stacks.iop.org/MST/15/254 (DOI: 10.1088/0957-0233/15/1/037)

Abstract

This paper presents a technique for measuring and quantifying the dielectrophoretic collection of sub-micron particles on planar microelectrode arrays. Fluorescence microscopy and video recording is used to measure the number of particles collecting on an electrode as a function of time for various experimental parameters, such as applied electrode voltage and frequency. Video images are processed using analytical methods that take advantage of the geometrical properties of the electrode array to extract quantitative information which is used to characterize the dielectric properties of particles. The time-dependent collection profiles can be characterized by three parameters: the initial dielectrophoretic collection rate, the initial to pseudo-steady-state transition and the rise time. This method can be used as a general technique to characterize the dielectrophoretic properties of populations of sub-micron-scale particles.

Keywords: non-uniform electric fields, particle concentration, dielectrophoretic collection, AC electrokinetics, Fokker–Planck equation, dielectrophoresis, interdigitated electrode array

1. Introduction

Novel electrokinetic methods for the non-contact manipulation of nanoscale particles in microfabricated structures are currently being explored by a number of groups worldwide (Morgan and Green 2003, Jones 1995). The future applications of this enabling technology are wide-ranging, particularly in biotechnology (Abramowitz 1996, Cheng *et al* 1998, Crippen *et al* 2000). In recent years, alternating current (AC) electrokinetic methods, such as electrorotation and dielectrophoresis (DEP), have been used to manipulate and separate many types of sub-micron particles with biological properties, including viruses, proteins, DNA and surface-modified latex microspheres (Cui *et al* 2001, Asbury *et al* 2002, Chou *et al* 2002).

DEP is the movement of polarizable particles in non-uniform electric fields (Pohl 1978). Particle forces arise from the application of an AC voltage to microelectrodes lying within a suspension of particles in a conducting fluid medium. The particles move under the influence of the non-uniform electric field, generated by the AC electrode potentials, depending on their effective polarizability. Positive DEP occurs when the effective polarizability of the particle is greater than the surrounding medium and particles move towards regions of high electric field non-uniformity. Electric field non-uniformities generated using planar interdigitated electrode arrays have the highest electric field gradients localized near the electrode edges. Consequently particles acting under a positive dielectrophoretic force accumulate on these planar interdigitated electrode edges, as shown in figure 1. The movement of the sub-micron-scale particles throughout the suspension is governed by deterministic dielectrophoretic forces and thermally driven stochastic fluctuations (Brownian

[1] Present address: School of Electronics and Computer Science, University of Southampton, Highfield, Southampton SO17 1BJ, UK.

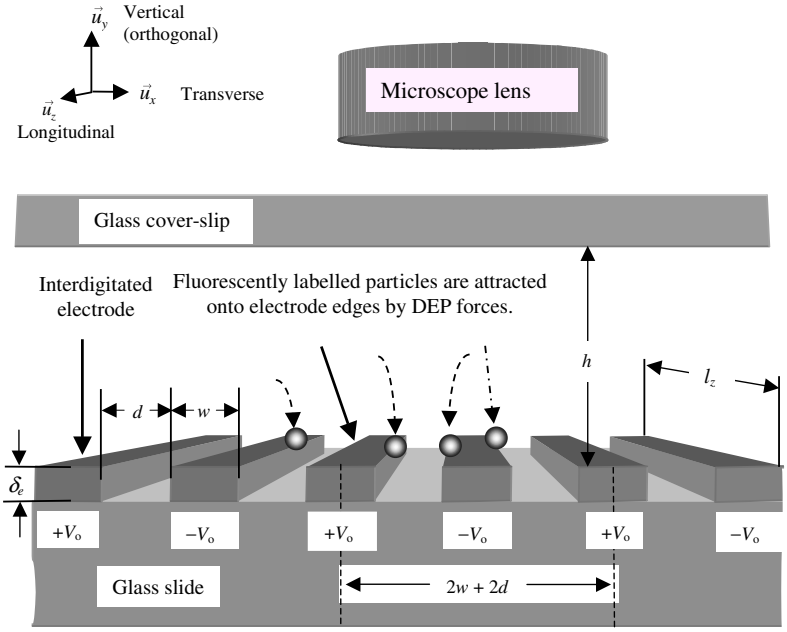

Figure 1. Diagram of a DEP collection experiment (using interdigitated electrodes fabricated on glass with width w, interelectrode spacing d and thickness δ_e) *not* to scale. The movement of the fluorescently labelled particles, suspended in an aqueous medium, is monitored with a microscope.

(This figure is in colour only in the electronic version)

motion). The time-dependent accumulation of particles near the electrodes is called the DEP *collection*. Conversely, particle movement away from the electrodes diffusing into solution after the DEP driving force has been switched off is called particle *relaxation*.

The application of DEP using planar electrodes means that the DEP forces are essentially short-ranged and ideal dielectrophoretic particle movement can be usefully described in several stages. Figure 2(a) depicts stages of an ideal DEP particle collection on a planar interdigitated electrode array:

(i) before DEP is switched on at $t = t_0$, where particles are uniformly distributed,
(ii) $t > t_0$ particles driven by DEP forces collect on electrodes, giving rise to a depletion zone above the array,
(iii) DEP forces continue to attract particles near the electrode surfaces, while above the depletion zone particles diffuse in so that the zone progressively moves away from the electrode surface, and
(iv) steady state, where DEP particle forces are balanced by diffusion ($t \to \infty$).

Two important parameters describing DEP collections (and relaxations) are, firstly, the initial time rate of increase in particles located near the electrodes or *collection rate* (immediately after the DEP force is switched on at $t = t_0$). This is illustrated by the dotted line in figure 2(b). Secondly, the change in particle collection between DEP being switched on and the steady state—called the initial to steady-state transition, which is also illustrated in figure 2(b) by ΔF (where F is the normalized fluorescence intensity, see equation (11)). The first experiments on the use of DEP collections for determining dielectric properties of particles were summarized by Pohl (1978). Subsequent measurements of time-dependent collections using optical absorption were reported by Talary and Pethig (1994) and Gascoyne *et al* (1994) who used the technique to measure the collections of cells and bacteria. Recently Milner *et al* (1998) and Suehiro *et al* (1999) also measured DEP collections using impedance methods. The latter developed a model which related the change in impedance to the cell concentration in an aqueous solution. However, very little work has been done in measuring and quantifying the time-dependent dielectrophoretic collection of sub-micron-scale particles on microelectrodes.

Asbury and co-workers (Asbury and van den Engh 1998, Asbury 1999, Asbury *et al* 2002) described measurements of the time-dependent DEP collection of DNA onto planar arrays and fitted these results by a single or double exponential profile. Their method quantitatively measured the peak values of the fluorescence near the electrode edges. These quantitative results of DNA trapping were performed at low AC frequencies ranging from ~10 Hz to 10 kHz (typically 30 Hz) and exhibited a dependence on electrolyte conductivity and on molecular weight. Fluorescence profiles of DNA being released and diffusing away from the electrode surfaces were also described.

In this paper we describe analytical methods for quantitatively determining DEP time-dependent collections based on fluorescence microscopy and describe the application of this method to quantifying the high frequency time-dependent collection of 216 nm diameter carboxyl-modified latex microspheres. Video images of the fluorescently labelled beads collecting onto 10 μm width 10 μm gap planar interdigitated arrays under the action of DEP were processed using MATLAB 5.0™ software routines based on these analytical methods. The software spatially averaged pixel values of sequential video frames, utilizing the symmetric and periodic structure of the interdigitated array design, to yield

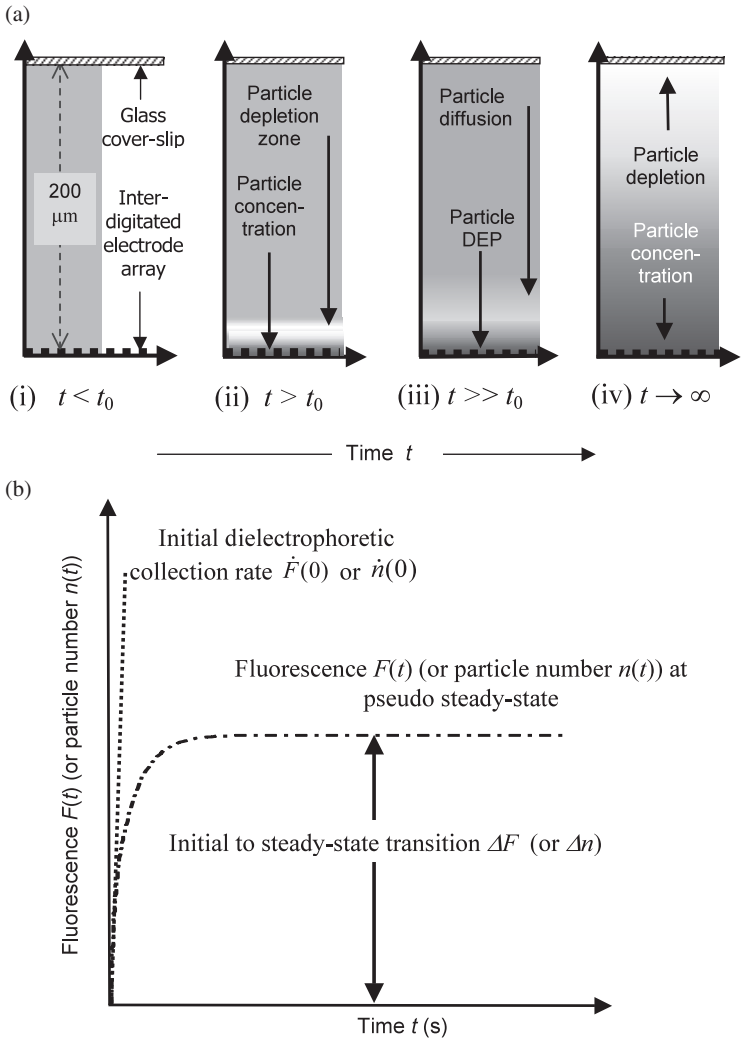

Figure 2. (a) Diagram illustrating the one-dimensional (1D) movement of particles between a glass cover slip (upper boundary) and planar interdigitated electrode array (lower boundary). (i) shows the distribution of particles before the onset of DEP at $t = t_0$, (ii) shows particle collection near the electrodes immediately after applying the DEP force ($t > t_0$) giving rise to the initial collection rate and a particle depletion zone above the array, (iii) shows continued particle collection at the electrodes ($t \gg t_0$) and the particle depletion zone moving upwards from the electrode plane, and (iv) shows the particle distribution at steady state ($t \to \infty$) where DEP particle forces are balanced by diffusion. (b) Graph of particle collection on the electrode array versus time corresponding to (a). The observed quantity is fluorescence $F(t)$ or particle number $n(t)$. The dielectrophoretic collection profiles for the arrangement can be described by the initial collection rate $\dot{F}(0)$ (or $\dot{n}(0)$) and the initial to pseudo steady-state change, ΔF (or Δn). The initial collection rate $\dot{n}(0)$ parameter (shown by the dotted line) pertains to times, $t > t_0$, very soon after the DEP force is switched on when particles collect near electrodes solely under the action of the DEP force. Much later, at $t \gg t_0$, the particle movement is governed by DEP and diffusion. At pseudo steady-state the movement by DEP is balanced by diffusion.

time-dependent fluorescent intensity profiles characterizing the particle collection around a representative electrode edge. The technique of spatially integrating particle fluorescence intensity around the electrode edges enables comparison of the particle collections with those predicted by theoretical simulations and can also be applied to fluorescently labelled DNA, viruses and proteins.

This paper also describes DEP collections for AC frequencies ranging from 0.5 to 5 MHz and extends the previous work of Bakewell and Morgan (2001) by including the electrical potential dependence of DEP collections for applied peak voltages $V_0 = 1$–4 V. The experimental results show that the dielectrophoretic response decreases as the frequency is increased and the voltage is reduced. These experimental observations are expected from the reduction in the effective polarizability predicted by the Clausius–Mossotti function and the square-law voltage dependence of the DEP force. Comparisons with trends predicted from computer simulations using a Fokker–Planck equation (FPE) model (Gardiner 1985) indicates that other effects, such as electrohydrodynamic fluid motion or changes to the field gradient due to particles collecting on the electrodes, contribute to the quantitative differences between theory and experiment. One consequence of these phenomena is that the particle concentration gradient at steady state is experimentally observed to be more uniform than predicted solely by DEP theory as illustrated in figure 2(a)(iv).

2. Theory

The FPE describes the behaviour, in space and time, of the concentration of particles in solution when subjected to an arbitrary external force. Under the influence of a time-averaged DEP force $\mathbf{F}_{\mathrm{DEP}}$ for non-interacting particles, the concentration c is related to the particle flux $\mathbf{J}$ by

$$\frac{\partial c}{\partial t} = -\nabla \cdot \mathbf{J} = -\frac{1}{\zeta}\nabla \cdot \left(c \underbrace{\frac{\alpha_{\mathrm{p}}}{4}\nabla |\mathbf{E}|^2}_{\mathbf{F}_{\mathrm{DEP}}} \right) + D\nabla \cdot \nabla c \qquad (1)$$

where α_{p} is the real part of the effective polarizability of the *particle* (or dipole moment per unit electric field), ∇ is the gradient operator, $\mathbf{E}$ is the electric field (peak value), ζ is the particle friction coefficient and D is the Boltzmann temperature-dependent diffusion constant, $D = k_{\mathrm{B}}T/\zeta$. It is understood $\mathbf{x} \equiv x, y, z$, $c \equiv c(\mathbf{x}, t)$, $\mathbf{J} \equiv \mathbf{J}(\mathbf{x}, t)$. For a spherical particle, $\alpha_{\mathrm{p}} = 4\pi r^3 \varepsilon_{\mathrm{m}} \mathrm{Re}\{f_{\mathrm{CM}}\}$, where $\mathrm{Re}\{f_{\mathrm{CM}}\}$ is the real part of the Clausius–Mossotti function, r is the particle radius and ε_{m} is the medium permittivity (Pohl 1978, Jones 1995, Morgan and Green 2003). Furthermore, the applied electrode voltage V_0 and electric field $\mathbf{E} \equiv \mathbf{E}(\mathbf{x})$ are related through $\mathbf{E} = V_0\mathbf{K}$, where $\mathbf{K}$ defines the relationship between the field and electrode geometry. The FPE can be solved numerically to give the particle concentration profile, provided that all the constants are known.

The DEP force on a particle is shown in equation (1) to depend on the effective polarizability α_{p} and the square of the electric field gradient, which can be calculated from the analytical solution to Laplace's equation for the interdigitated electrodes (Morgan *et al* 2001). The FPE can be simplified to a two-dimensional (2D) problem for the interdigitated electrode array shown in figure 1, where the electrodes are considered to be infinitely long and therefore end effects can be ignored.

The time-dependent accumulation of particles, or *collection profile*, for the FPE reduced to 2D is given by the particle number $n(t)$ per unit longitudinal length, which is related to the concentration over a cross sectional area A:

$$n(t) = \int_{\mathrm{A}}\int c(\mathbf{x}, t)\,\mathrm{d}\mathbf{x} = \int_{x_1}^{x_2}\int_{y_1}^{y_2} c(x, y, t)\,\mathrm{d}x\,\mathrm{d}y. \qquad (2)$$

An expression for the *initial* collection rate of particles $\dot{n}(0)$ ($\cdot$ denotes time derivative) arriving at the electrodes can be determined by assuming the initial particle concentration to be uniform throughout the volume, implying, at $t = 0$, $\nabla c = 0 = \nabla^2 c$. The initial collection rate is approximately proportional to the DEP force and can be used as a measure of the dielectric properties of the particles. Combining equations (1) and (2), it can be shown $\dot{n}(0) \propto \alpha_{\mathrm{p}} V_0^2 n(0)/\zeta$, where V_0 is the applied electrode voltage (peak) and $n(0)$ is the initial number of particles. Thus, two collection experiments (labelled '1' and '2') using the same electrode array, ζ, $n(0)$, etc, but assuming *separate* parameter values for V_0 and α_{p}, will have theoretically predicted collection ratios

$$\frac{\dot{n}_2(0)}{\dot{n}_1(0)} = \frac{\alpha_{\mathrm{p}_2} V_{0_2}^2}{\alpha_{\mathrm{p}_1} V_{0_1}^2}. \qquad (3)$$

The steady-state distribution of the particles occurs as $t \to \infty$ and is governed by the balance of fluxes (DEP and diffusion). This is found by solving equation (1) with $\partial c/\partial t = 0$. The ratios of steady-state particle concentration for two collection experiments with separate parameter values for V_0 and α_{p} are

$$\frac{c_2(x, y, \infty)}{c_1(x, y, \infty)} = C \exp\left(\frac{1}{4k_{\mathrm{B}}T}(\alpha_{\mathrm{p}_2} V_{0_2}^2 - \alpha_{\mathrm{p}_1} V_{0_1}^2)|\mathbf{K}(x, y)|^2 \right) \qquad (4)$$

where C is an arbitrary integration constant.

3. Experimental materials and methods

To perform a typical DEP particle collection experiment, 40 μl of a fluorescently labelled 216 nm diameter bead suspension was micro-pipetted into the electrode array well. A 18 × 18 mm^2 cover slip was placed over the suspension to reduce evaporation and to enable the array to be viewed under a microscope, as shown schematically in figure 1. The DEP experiment was recorded using a CCD camera (not shown) set with automatic gain control turned off. The video images were of the planar electrode array, of area ≅190 μm × 250 μm.

3.1. Planar interdigitated electrode arrays

The planar interdigitated electrodes, shown in figure 1, were fabricated on glass microscope slides using standard positive S1818 resist photolithography and metallic vapour deposition techniques (Pacansky and Lyerla 1979). The Ti–Pd–Au electrodes had thickness $\delta_{\mathrm{e}} = 120$ nm, width $= w = 10$ μm, gap $= d = 10$ μm and length $l_z \cong 2$ mm. Eight separately addressable electrode arrays were fabricated on a slide spanning a total rectangular planar area of 200 mm^2. Two narrow cover slips, fixed along the long sides of the rectangular 8-electrode array, enabled the height h of the 18×18 mm^2 cover slip above the electrode plane to be well controlled. Using a 40 μl microsphere droplet resulted in $h \cong 200$ μm.

The electrode arrays fabricated on glass were in turn mounted on a printed circuit board. As indicated in figure 1, neighbouring electrodes in the array were supplied with electrical potentials of opposite ($\pm V_0$) polarity. The frequency and voltage supplied to the electrodes was controlled by a digital data synthesizer (DDS) and the electrode potentials were switched on/off manually and monitored by an oscilloscope.

3.2. Preparations of latex microspheres and experimental measurements

The model colloidal particles used for DEP experiments were 216 nm diameter carboxyl-modified polystyrene fluorescent microspheres FluoSpheres® (Molecular Probes, Eugene, USA, F-8811) with yellow–green emission wavelength of 515 nm. The 216 nm diameter latex microspheres were supplied as 2% solids (w/w) in aqueous solution (2 mM sodium azide in distilled water). Stock preparations of the microspheres consisted of 1 μl of 2% solids added to distilled RO water to make a final volume of 100 μl. In each experiment, 4 μl of this stock was added to 36 μl dilute KCl solution to give a final bead dilution of 1:1000. The measured conductivity of the

microsphere suspension was $\sigma_m = 1.7$ mS m^{-1} (Jenway 4701, RS Components, UK). Assuming the density of polystyrene is 1.05 g cm^{-3} the final microsphere concentration used at the start of the DEP experiments was estimated as $c_V = 3.613 \times 10^{15}$ m^{-3} or $c_V \cong 4 \times 10^{-3}$ μm^{-3} (Bangs 1997). This value approximately agreed with the number of beads visible over the planar array before the onset of DEP, assuming a 1 μm vertical depth-of-focus.

3.3. Development of video image processing software

Figure 3 shows typical recorded video images of a DEP experiment before and after applying the electric field. Both images are approximately half-length frame size (540 × 360 pixels) and have been cropped and juxtaposed for illustrative purposes. Figure 3(a) shows the planar interdigitated array before application of the electric potential where particles exhibit Brownian motion in the suspending medium. This corresponds to figure 2(a)(i). Figure 3(b) shows particle collection in the immediate vicinity of the electrodes under the action of positive DEP about five seconds after applying the field. The particle concentration in the plane immediately above the electrodes is depleted—as depicted in figure 2(a)(ii). The time-dependent particle concentration on the electrodes is determined by experimental conditions, in particular the polarizability which is a function of frequency. Consequently, an accurate measurement of bead concentration as a function of time should enable a quantification of the frequency-dependent DEP force.

In order to achieve quantitative evaluation we have developed the following image processing technique outlined schematically in figure 4. Video footage is captured using a miroVIDEO® DC 30 (CA, USA) frame grabber and converted by Photo-Paint 6.0® (Corel, CA, USA) from an AVI file to either a sequence of TIFF images or a MPEG movie file (Haskell *et al* 1997), as indicated in figure 4. The capture rate ranges from 1 to 25 frames s^{-1}. A time-dependent fluorescence profile of the collection experiment is constructed by sequentially image processing each frame automatically using a user-interactive program written in MATLAB 5.0™ (programs available from the author). The image processing takes advantage of the transverse periodicity and symmetry of the array. Figure 4 outlines the conversion of the time sequence of video image intensities recorded from the camera, written as $I(x', z', t)$, to the fluorescence intensity $F(t)$ representing DEP particle collection near a representative electrode edge. A key intermediate step is the transformation of the 2D intensity of each frame to a 1D intensity plot with transverse dimensions periodically and symmetrically averaged to an electrode half-width and half-gap $(w/2 + d/2)$. This intensity, representing the fluorescence of the array, is called a *characteristic* intensity, $\tilde{I}(x, t)$ (written in discrete form as $\tilde{I}(i, t)$) and can be evaluated as a function of time and experimental conditions, such as frequency and voltage.

A simpler method of quantifying particle collection using fluorescence microscopy was demonstrated by Asbury and van den Engh (1998) and Asbury (1999). These authors quantified DNA collection by averaging the height of the fluorescence signal from each electrode strip. We have extended this procedure and integrated the signal in a well-defined region either side of the electrode edge (i.e. in the transverse direction). Relating time-dependent particle collection to the area of the fluorescent signal has the advantage of being able to directly quantify the number of particles in a defined region on the electrodes and facilitates a more accurate comparison with simulation.

3.3.1. Image processing set-up—array geometry. Each frame is processed automatically to generate a time-dependent particle collection profile. In order to set up the automated frame processing, data are entered into the software about the geometry of the array using a sample of TIFF images for 'training' the program, as outlined in figure 4. To ensure correct alignment for pixel averaging the image was often rotated, typically through an angle $-0.3° \leqslant \theta \leqslant 0.3°$, since an angular error of 0.1° over 720 pixels horizontally resulted in a mismatch of approximately 1 pixel in the 'vertical' axis of the screen image. Figure 5(a) shows a rotated video frame of a DEP collection, cropped for illustration, where the angular alignment of the electrode edges concurs with the horizontal axis of the screen.

To construct the characteristic intensity $\tilde{I}(r, t)$ for an electrode half-width and half-gap $(w/2 + d/2)$, each electrode and neighbouring gap is paired and the number of electrode-gap pairs, n_{pr}, is selected in the program. The number of edges is $n_{ed} = 2n_{pr} + 2$. In figure 5(a) the transverse position of the first and last electrode edges is denoted as x_a and x_b. The number of pairs and edges in this figure is $n_{pr} = 8$ and $n_{ed} = 18$. The location of electrode edges in the transverse direction is entered by visual inspection using the mouse-controlled hairline. Each registered location is shown by the cross, '+', marker superimposed on the image in figure 5(a) and is written as $x_+(k)$, where $k \in [1, n_{ed}]$. The number of pixels between electrode edges varies by as much ±5% whereas the electrode dimensions are known to remain constant, $w = d = 10$ μm. To circumvent this problem, the longitudinally averaged intensity is re-sampled such that each electrode width and gap between x_a and x_b receives the same number of samples. The number of sample points for $w/2 = d/2$ is given by $n_{1/2}$. Hence the number of sample points for each $w/2 + d/2$ *characteristic* is therefore $n_c = 2n_{1/2}$. Typically, $30 \leqslant n_{1/2} \leqslant 50$. Parameter values for θ, n_c, $x_+(k)$ and internal program flags are stored for use in automated processing, as indicated in figure 4.

3.3.2. Multiple image processing and fluorescence intensity. The plane of the 2D image at the camera, $I(x', z', t)$, is assumed to be parallel to the plane of the electrodes and spans directions $\vec{u}_{x'}$ and $\vec{u}_{z'}$. The first three automated image processing steps use the longitudinal and transverse periodic and symmetric properties of the array to construct the characteristic $w/2 + d/2$ intensity, $\tilde{I}(x, t)$. The fourth step averages over a short transverse segment in the vicinity of the electrode edge, thus representing 'particle collection' for the imaged array at a particular instant in time. The steps are listed in figure 4: (i) 2D image rotation, (ii) longitudinal average, (iii) transverse re-sampling, segmentation, periodic and symmetric average and (iv) transverse average about the electrode edge. The details are as follows:

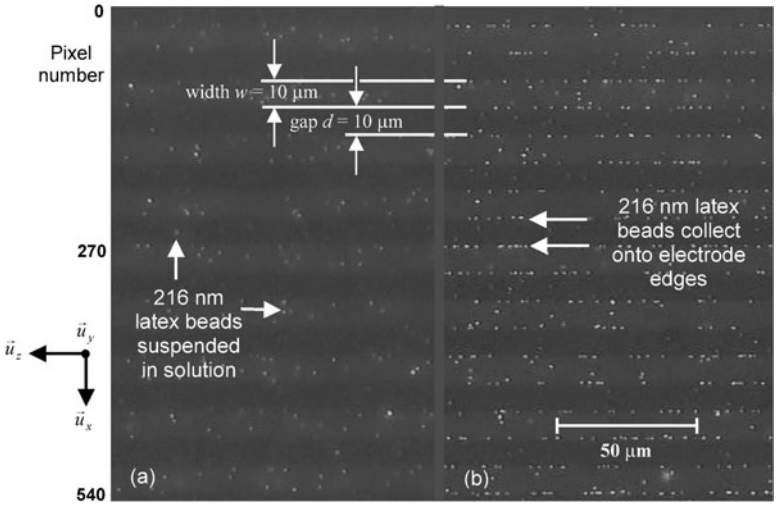

Figure 3. Positive DEP collection of 216 nm diameter fluorescent microspheres onto $d = w = 10\ \mu$m interdigitated electrodes (a) ~1 s before the DEP force was applied (b) ~5 s after the DEP force was applied.

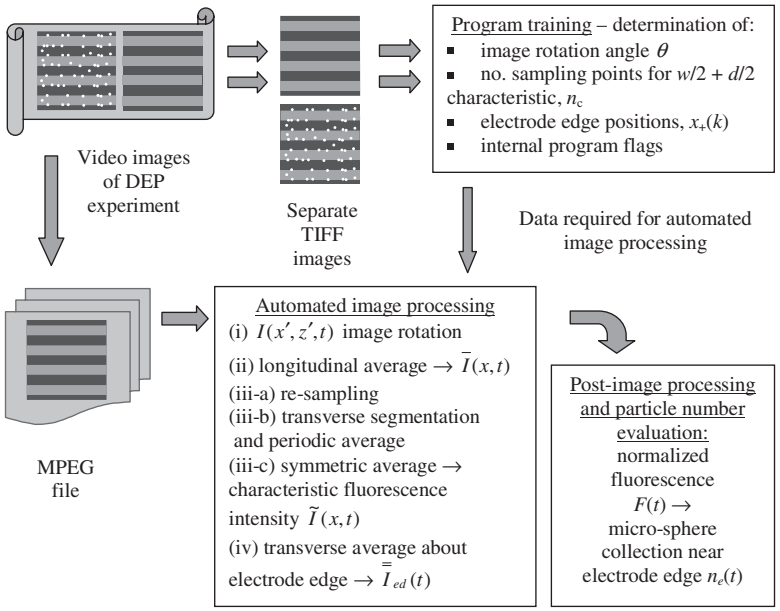

Figure 4. Schematic of image processing software that converts the 2D fluorescence intensity $I(x', z', t)$ recorded in each video frame to normalized fluorescence $F(t)$ representing DEP particle collections (and relaxations) in the near vicinity of a electrode edge representative of the interdigitated electrode array.

(i) Each frame is either a TIFF image, or decoded MPEG image, and is rotated by θ such that $I(x', z', t) \rightarrow I(x, z, t)$, where θ is specified by the training program described in the previous section. The rotated image, $I(x, z, t)$, is written in discrete form $I(r, c, t)$ suitable for pixel averaging, where r and c are respectively pixel values for each row r and column c.

(ii) The longitudinal fluorescence intensity average along the columns c for each pixel location (row r) in the transverse direction is given by

$$\bar{I}(r,t) \cong \Delta z \sum_{c=1}^{c_{\max}} I(r,c,t) \Big/ \Delta z \sum_{c=1}^{c_{\max}} 1 = \frac{1}{c_{\max}} \sum_{c=1}^{c_{\max}} I(r,c,t) \qquad (5)$$

where Δz is the finite differential increment along the longitudinal direction, $\vec{u}_z$, and $c_{\max} = 720$ is the total number of column pixels. A plot of the average intensity $\bar{I}(r, t_i)$ extracted from the program for the example greyscale frame of figure 5(a) is shown in 5(b). The plot shows the presence of beads at the edges corresponds to peaks in the average intensity and the values are generally higher over the gold electrodes than the gaps since the former reflect more scattered light.

(iii) (a) Re-sampling of the longitudinally averaged intensity $\bar{I}(r, t)$ is performed by the following mapping:

$$\underbrace{\bar{I}(r,t)}_{\text{Intensity}} \rightarrow \underbrace{\bar{I}(x,t)}_{\text{Interpolate}} \rightarrow \underbrace{\bar{I}(x_s,t)}_{\text{Resample}} \rightarrow \underbrace{\bar{I}(j,t)}_{\text{Reconstructed Intensity}} . \qquad (6a)$$

The pointer $x_s(j)$, with $j = n_c(k-1) + i$, $k =$

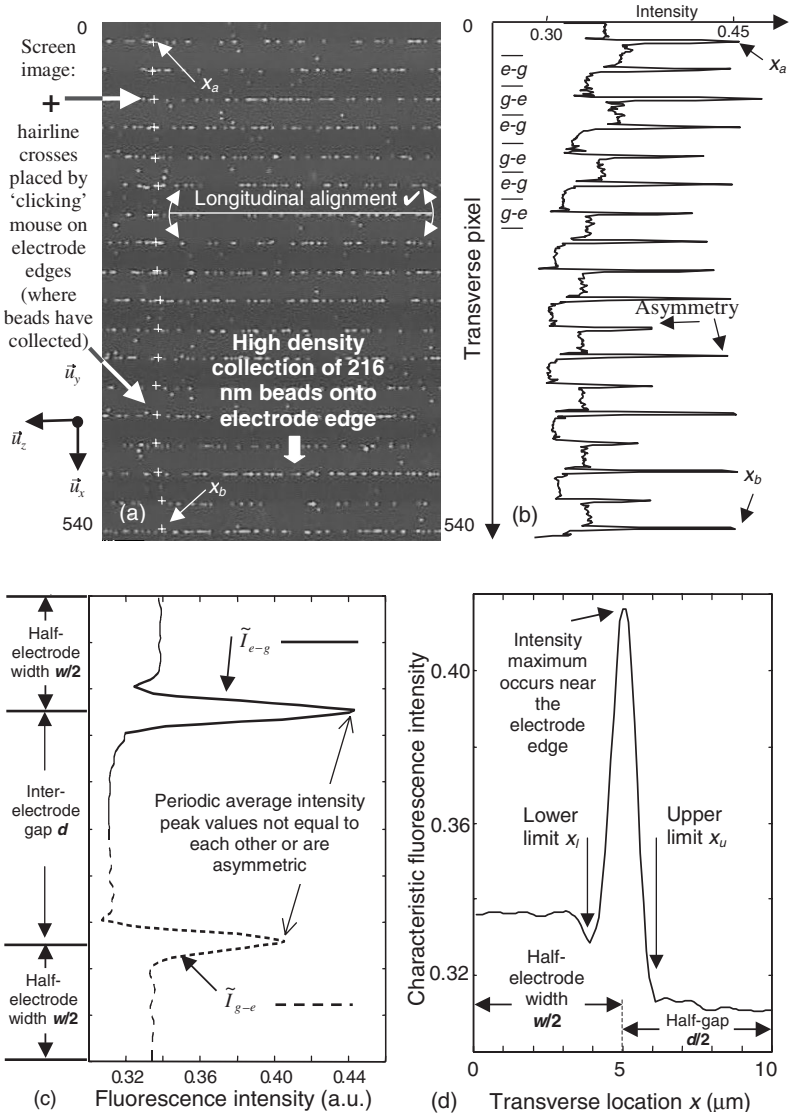

Figure 5. (a) Positive DEP collection image processed frame (37 s after DEP force applied) with (b) associated average longitudinal greyscale intensity for each transverse pixel. (c) is the periodic average of the fluorescence intensity for $\tilde{I}_{\mathrm{e-g}}(x,t)$ (——) and $\tilde{I}_{\mathrm{g-e}}(x,t)$ (— — —) for the two segment types shown in (b). The symmetric average of $\tilde{I}_{\mathrm{e-g}}$ and $\tilde{I}_{\mathrm{g-e}}$ is the $w/2+d/2$ *characteristic* intensity $\tilde{I}(x,t)$, (d), that represents the pixel intensity for the entire video frame.

$\{1,2,\ldots,n_{\mathrm{ed}}-1\}$ and $i=\{1,2,\ldots,n_{\mathrm{c}}\}$ assigns transverse locations where the interpolated intensity $\bar{I}(x,t)$ is re-sampled at locations

$$x_{\mathrm{s}}(j)=x_{+}(k)+i[x_{+}(k+1)-x_{+}(k)]/n_{\mathrm{c}}. \qquad (6b)$$

(b) To construct the $w/2+d/2$ characteristic intensity, the fluorescence profile in the transverse direction between x_a and x_b is segmented into two transverse types and averaged. Several examples are illustrated in figure 5(b), the segments labelled 'e–g' signify pixels located within the transition from electrode half-width to half-gap (moving down figure 5(b) from x_a to x_b), and the segments labelled 'g–e' signify pixels lying within the transition from half-gap to electrode half-width. The intensities along each of the two segment types are averaged over the electrode and gap pairs n_{pr} according to

$$\underbrace{\tilde{I}(i,t)}_{\tilde{I}_{\mathrm{e-g}}}=\frac{1}{n_{\mathrm{pr}}}\sum_{k=1}^{n_{\mathrm{pr}}}\underbrace{\bar{I}(i+n_{1/2}+2n_{\mathrm{c}}(k-1),t)}_{I_{\mathrm{e-g\ segments}}}$$
$$\forall\, i=\{1,2,\ldots,n_{\mathrm{c}}\} \qquad (7a)$$

$$\underbrace{\tilde{I}(i+n_{\mathrm{c}},t)}_{\tilde{I}_{\mathrm{g-e}}}=\frac{1}{n_{\mathrm{pr}}}\sum_{k=1}^{n_{\mathrm{pr}}}\underbrace{\bar{I}(\mathrm{i}+n_{1/2}+2n_{\mathrm{c}}(k-1)+n_{\mathrm{c}},t)}_{I_{\mathrm{g-e\ segments}}}$$
$$\forall\, i=\{1,2,\ldots,n_{\mathrm{c}}\} \qquad (7b)$$

where the *tilda* symbol ($\sim$) denotes a 'periodic' *average* profile spanning the interval $w/2+d+w/2$ (one electrode width and gap) and subscripts 'e–g' and 'g–e' correspond to the examples in figure 5(b). The $n_{1/2}$ end segments are not included (as shown). The periodic average for the longitudinally averaged intensity, figure 5(b), is shown in 5(c) for $i=\{1,2,\ldots,2n_{\mathrm{c}}\}$ and $n_{\mathrm{c}}=100$.

The variation of the peak intensities in figure 5(b) is approximately proportional to the number of beads accumulated at each of the electrode edges. Some of the intensities at the edges showed a marked asymmetry, as depicted in figure 5(b), and are clearly shown in the periodic average, figure 5(c). This is not expected from the theory that predicts the DEP force and hence particle collection (for positive DEP) on both sides of any electrode edge should be the same. Fluctuations similar to these have been reported by other workers (Asbury and van den Engh 1998).

(c) The symmetric average is obtained by rotating the $\tilde{I}_{\mathrm{g-e}}$ profile by 180°, as shown in figure 5(c), and superimposing onto the $\tilde{I}_{\mathrm{e-g}}$ profile. The average yields the *characteristic* intensity $\tilde{I}(x,t)$, written in *discrete* form as $\tilde{I}(i,t)$:

$$\tilde{I}(i,t) = \tfrac{1}{2}\Big[\underbrace{\tilde{I}(i,t)}_{I_{\mathrm{e-g}}} + \underbrace{\tilde{I}(2n_{\mathrm{c}}+1-i,t)}_{I_{\mathrm{g-e}}\ \text{rotated}\ 180^{\circ}}\Big] \qquad \forall\, i = \{1,2,\ldots,n_{\mathrm{c}}\}. \tag{8}$$

The $\tilde{I}(i,t)$ for the example in figures 5(a)–(c) is shown in figure 5(d) (redrawn with the transverse axis horizontal). $\tilde{I}(i,t)$ is called the *characteristic* intensity since it represents the average intensity along $\vec{u}_z$ and the periodic and symmetric average across $\vec{u}_x$. The periodic and symmetric properties of the array enables the transverse region $\vec{u}_x$ to be divided into 'cells'. Thus $\tilde{I}(i,t)$ spans $0 \leqslant x \leqslant x_{\mathrm{c}}$, where $x_{\mathrm{c}} = \frac{w+d}{2}$. Figure 5(d) shows the peak of the intensity due to bead accumulation is located close to the electrode edge, positioned at $x_{\mathrm{e}} = \frac{w}{2}$. The time-dependent $w/2+d/2$ fluorescence intensity characteristic, $\tilde{I}(i,t)$, is stored as a matrix where each row represents a time 'slice' at $t = t_j$, the first column is the time (s) and the remaining columns are the associated intensity profiles. An example of a 3D plot of the matrix resulting from particle collection for the $w/2+d/2$ transverse interval is shown in figure 6.

(iv) The time-dependent intensity profile for particle accumulation is determined from the characteristic intensity $\tilde{I}(x,t)$ by averaging in the transverse direction $\vec{u}_x$ typically for a small region of interest centred about the electrode edge, x_{e}. This interval is specified by x_{u}–x_{l}, where x_{l} and x_{u} are the lower and upper limits illustrated in figure 5(d) and are related to the integer values i_{l} and i_{u}: $x_{\mathrm{l}} = (i_{\mathrm{l}}-1)\Delta x = (i_{\mathrm{l}}-1)(\frac{w+d}{2})/(n_{\mathrm{c}}-1)$, $x_{\mathrm{u}} = (i_{\mathrm{u}}-1)\Delta x = (i_{\mathrm{u}}-1)(\frac{w+d}{2})/(n_{\mathrm{c}}-1)$, with Δx the finite differential increment along the transverse direction, $\vec{u}_x$.

The average of $\tilde{I}(x,t)$ over x_{u}–x_{l} is evaluated using the trapezium rule:

$$\bar{\bar{I}}_{\mathrm{ed}}(t) = \int_{x_{\mathrm{l}}}^{x_{\mathrm{u}}} \tilde{I}(x,t)\,\mathrm{d}x \Big/ \int_{x_{\mathrm{l}}}^{x_{\mathrm{u}}} \mathrm{d}x \cong \frac{\hat{I}_{\mathrm{ed}}(t)}{i_{\mathrm{u}}-i_{\mathrm{l}}} = \frac{1}{i_{\mathrm{u}}-i_{\mathrm{l}}}\left[\frac{\tilde{I}(i_{\mathrm{l}},t)+\tilde{I}(i_{\mathrm{u}},t)}{2} + \sum_{i=i_{\mathrm{l}}+1}^{i_{\mathrm{u}}-1}\tilde{I}(i,t)\right] \tag{9}$$

where the subscript 'ed' denotes the average is over the transverse interval 'in the near vicinity of the electrode edge' and the double overbar denotes spatial averages in both directions $\vec{u}_x$ and $\vec{u}_z$. If the limits are reasonably close to the electrode edge $x_{\mathrm{e}} = \frac{w}{2}$, but not too close, the integral is a measure of the fluorescence intensity of particles located 'about the electrode edge'. If x_{l} is too low and x_{u} too high, the change in intensity 'about the electrode edge' is poorly represented. On the other hand, if x_{l} and x_{u} are close to each other at the edge, $x_{\mathrm{e}} = \frac{w}{2}$, the integral $I_{\mathrm{ed}}(t_i)$ is prone to changes in the precise shape of $\tilde{I}(x,t)$. Small changes in the shape of $\tilde{I}(x,t)$ can occur due to misjudgements of the position of the electrode edges during image processing set-up.

3.3.3. Post-image processing: normalized fluorescence intensity. Fluctuations in the fluorescent light source often occur with mercury lamps (Ploem and Tanke 1987) which results in small-time variations in $I_{\mathrm{ed}}(t)$. These fluctuations can be smoothed by normalizing $I_{\mathrm{ed}}(t)$ with respect to the average intensity $\tilde{I}(i,t)$ representing the entire $w/2 + d/2$ transverse interval. This is the *total* intensity, $\bar{\bar{I}}_{\mathrm{T}}(i,t)$:

$$\bar{\bar{I}}_{\mathrm{T}}(t) = \frac{\hat{I}_{\mathrm{T}}(t)}{n_{\mathrm{c}}-1} = \frac{1}{n_{\mathrm{c}}-1}\left[\frac{\tilde{I}(1,t)+\tilde{I}(n_{\mathrm{c}},t)}{2} + \sum_{i=2}^{n_{\mathrm{c}}-1}\tilde{I}(i,t)\right]. \tag{10}$$

The normalized intensity can be found by dividing equations (9) by (10) and this approach is suitable, for example, for dielectrophoretic measurements of DNA collecting over the interelectrode gap (Bakewell 2002). For colloidal particles collecting near the electrode edges, the normalized fluorescence intensity $F(t)$ is more suitably expressed in terms of $\bar{\bar{I}}_{\mathrm{ed}}(t)$ and $\bar{\bar{I}}_{\mathrm{lu}}(t)$, which is the average intensity for the x intervals *away* from the edge, $0 \leqslant x \leqslant x_{\mathrm{l}}$ and $x_{\mathrm{u}} \leqslant x \leqslant \frac{w+d}{2}$:

$$F(t) = \frac{\bar{\bar{I}}_{\mathrm{ed}}(t)}{\bar{\bar{I}}_{\mathrm{lu}}(t)} = \frac{\hat{I}_{\mathrm{ed}}(t)/[i_{\mathrm{u}}-i_{\mathrm{l}}]}{[\hat{I}_{\mathrm{T}}(t)-\hat{I}_{\mathrm{ed}}(t)]/[i_{\mathrm{l}}-1+n_{\mathrm{c}}-i_{\mathrm{u}}]} \tag{11}$$

where $\hat{I}_{\mathrm{ed}}(t)$ and $\hat{I}_{\mathrm{T}}(t)$ are given by equations (9) and (10). The post-image processing step of fluorescence normalization is indicated in figure 4 and an example of $F(t)$ evaluated using $\tilde{I}(x,t)$, shown in figure 6, is illustrated in figure 7. In general, normalization tends to increase the sensitivity of the rise profile and in the hypothetical case, where particle collection onto the electrode edge causes almost entire particle depletion elsewhere such that $\bar{\bar{I}}_{\mathrm{ed}}(t) \neq 0$ and $\bar{\bar{I}}_{\mathrm{lu}}(t) \to 0$, then $F(t) \to \infty$. In practice, DEP experiments do not exhibit extreme particle depletion, except when the aqueous suspending medium has almost entirely evaporated, so (11) is satisfactory to use.

3.3.4. Determining DEP collections from normalized fluorescence intensity. The fluorescence intensity, $\bar{\bar{I}}_{\mathrm{ed}}(t)$ can be written in terms of the fluorescence from particles within a small $\approx$1 μm vertical depth-of-focus (located close to the electrode plane) and fluorescence from particles above the focal plane in the bulk solution. A similar phenomenological model for $\bar{\bar{I}}_{\mathrm{lu}}(t)$ can also be written. Combining both expressions using (11), the temporal change in normalized fluorescence for the DEP collection time interval t–t_0 is

$$\Delta F(t) = F(t) - F(t_0) = k[n_{\mathrm{e}}(t) - n_{\mathrm{e}}(t_0)] + \varepsilon_f(t) = k\Delta n_{\mathrm{e}}(t) + \varepsilon_f(t) \tag{12}$$

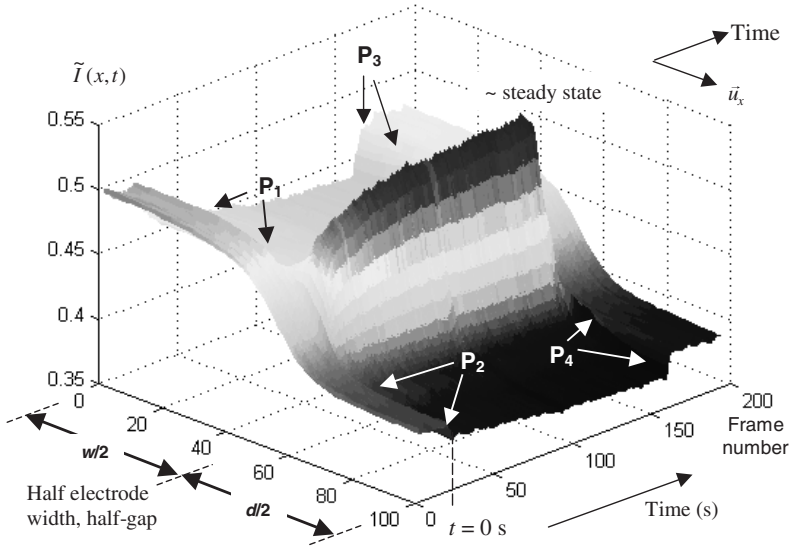

Figure 6. Example of a characteristic $w/2 + d/2$ fluorescence intensity $\tilde{I}(x, t)$ of a sequence of video frames that shows DEP particle collection and relaxation about a representative electrode edge for the experimental condition, $V_0 = 2$ V, $f = 1$ MHz.

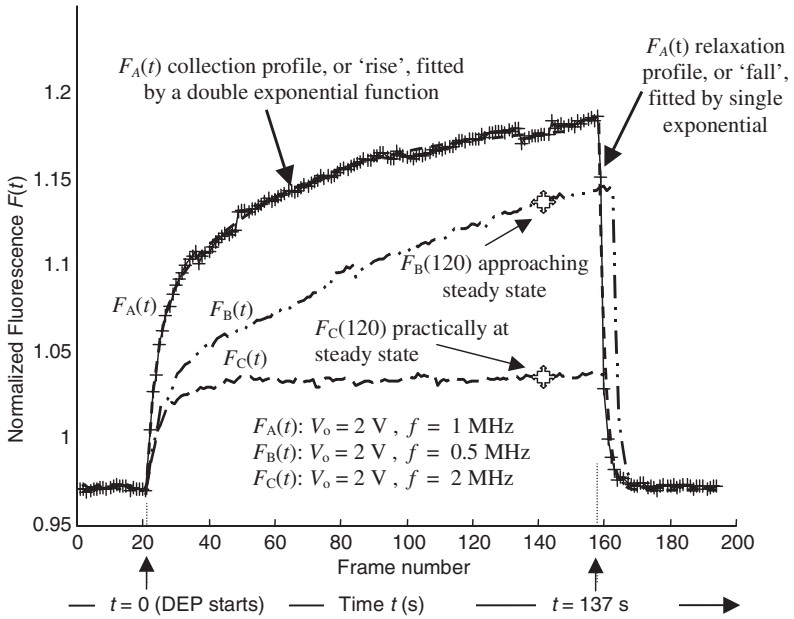

Figure 7. Examples of normalized fluorescence $F(t)$ for DEP collections and relaxations for different experimental conditions. The $F_A(t)$ collection and relaxation profile was evaluated from $\tilde{I}(x, t)$, illustrated in figure 6.

where $n_e(t)$ is the number of particles at an electrode edge of a representative cell for $x_l \leqslant x \leqslant x_u$, k is a constant and the error is ε_f. The subscript 'e' denotes the particle number is determined by *experiment* via ΔF and the particles are in the near vicinity of the electrode *edge*. The constant k includes optical parameters such as the numerical aperture of the objective, re-absorption of emitted light, quantum efficiency of the fluorophore, absorption, scattering and excitation absorbance. The constant also includes the effect of fluorescence in the transverse region away from the edge, $0 \leqslant x \leqslant x_l$ and $x_u \leqslant x \leqslant x_c$, which is assumed to remain unchanged during the course of the experiment.

Essentially, the background fluorescence within the plane of focus is eliminated by assuming it remains unchanged for $t > t_0$. The error term ε_f accounts for any deviation from these together with other assumptions and is typically small, $\varepsilon_f(t) < 0.1k\Delta n_e(t)$. This means the difference in normalized fluorescence about the electrode edge is approximately proportional to the difference in particle concentration near the edge. Re-arranging (12), and without loss of generality setting $t_0 = 0$, at time t the change in particle number located near the electrode is approximated by

$$\Delta n_e(t) = [\Delta F(t) - \varepsilon_f(t)]/k \cong \Delta F(t)/k. \qquad (13)$$

A value for k is found experimentally by counting the number of beads along the electrode edges and comparing it with the measured fluorescence for selected frames (or times $t = t_j$) during DEP collection. The relation between ΔF and Δn_e

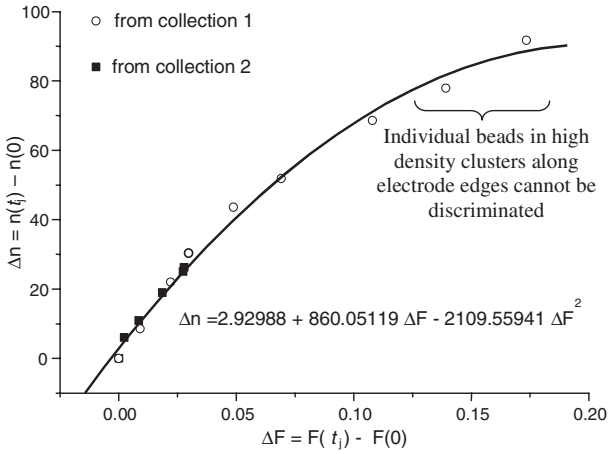

Figure 8. Relationship between the change in average bead number Δn_e (collected on the electrode edges) and change in fluorescence ΔF.

is mapped in figure 8 for two sets of data and was fitted to a second-order polynomial using Origin 4.1™. The relationship between Δn_e and ΔF is linear for low Δn_e. For high ΔF, however, individual beads lying on the electrode edges in groups or clusters are practically impossible to distinguish. Therefore, the value of the constant was taken from the linear term in the polynomial, $k = 1/860$.

Considering infinitesimal time increments, $t = t_0 + \Delta t$ and taking limits $\Delta t \to 0^+$, (13) leads to

$$\dot{n}_e(0) = \dot{F}(0)/k \tag{14}$$

where the dot '·' denotes the time derivative and is understood to be in the $+t$ direction at $t_0 = 0$. Experimental values for the initial particle collection rate can be estimated by measuring the gradient of F over small increments in time immediately before and after the DEP force is applied, $\dot{F}(0) \cong \delta F/\delta t$. An alternative and more robust method deduces $\dot{F}(0)$ from the entire collection characteristic, $F(t)$. The characteristic is fitted to an analytical function, typically a double exponential, and the function is differentiated with respect to time. The equation for the DEP collection starting at $t = t_0$ suitable for fitting with commercially available software, such as Origin 4.1™, has the form

$$F(t) = F_0 - F_1 \exp[-(t - t_0)/\tau_{e1}] - F_2 \exp[-(t - t_0)/\tau_{e2}] \tag{15}$$

where τ_{e1} and τ_{e2} are the rise times and components $F_1 > 0$ and $F_2 > 0$. Differentiating with respect to time, setting $t = t_0 = 0$ and using (14), the initial collection rate is given by

$$\dot{n}_e(0) = \frac{\dot{F}(0)}{k} = \frac{F_1/\tau_{e1} + F_2/\tau_{e2}}{k}. \tag{16}$$

4. Results and discussion

The DEP collections and relaxations for the 216 nm diameter fluorescently labelled microspheres were investigated for two *independent* variables: applied DEP frequency, f, and peak potential, V_0. Three different frequencies were applied using $V_0 = 2$ V: $f = 500$ kHz, 1 MHz, and 2 MHz. No collections were observed for $f \geqslant 3$ MHz. Collections using three peak voltages, $V_0 = 1$, 2 and 4 V, were conducted at $f = 2$ MHz. In each experiment the particle *collection* was observed for 2–3 min, followed by particle *relaxation* (DEP switched off, $V_0 = 0$ V), which was observed for 30–60 s.

Since particle collections tended to vary over the area of an array, collections and relaxations were performed in *sets* of *three* experiments. In each set, the same area of the array was used to record particle collections (and relaxations) for all of the three possible *states* of the independent variable (f or V_0). This enabled the collections to be compared with each other to avoid, as far as possible, any disparities in bead density arising from variations in electrode edge definition during micro-fabrication.

4.1. An example of DEP collection and relaxation

A typical characteristic intensity $\tilde{I}(x, t)$ is illustrated in figure 6 for a 216 nm diameter fluorescent bead DEP collection on the planar interdigitated electrode array described in section 2 with experimental conditions $V_0 = 2$ V and $f = 1$ MHz. The characteristic was generated using expressions (5)–(8). The first feature of $\tilde{I}(x, t)$ is that 2 min after the onset of DEP, the collection over the electrode edge is substantially at a steady state. The video was frame grabbed at a rate of 1 frame s^{-1}, so the entire collection and relaxation required about 200 frames to image process.

The second feature of figure 6 is that a small decrease in fluorescence occurs over the lower and upper transverse intervals after the onset of DEP ($t = 0$ s), at points located near P_1 and P_2. The precise cause of this reduction is not entirely clear but it generally occurs with all DEP experiments, so it is not attributed to fluctuations in the source intensity. Restoration of the fluorescence also occurs after the DEP is switched off, as shown near points P_3 and P_4. The fluorescence reduction (and restoration) phenomena tend to be more pronounced when the DEP force is strong, so it is likely to be due to DEP-induced depletion of particles within and above the focal plane. Fluorescence depletion and restoration affects no more than about 10% of the intensity $\tilde{I}(x, t)$ so the approximation for the error $\varepsilon_f(t)$ in (13) applies. As shown in figures 5(a)–(d) the intensity is slightly higher over the (gold) electrode than the (glass) gap since the former reflects more light. Small temporal variations in the source are evident and can be minimized or cancelled by normalization.

Spatially averaging and normalizing $\tilde{I}(x, t)$ using equations (9)–(11) led to a collection and relaxation normalized fluorescence profile, $F_A(t)$, shown in figure 7. The data points (denoted '+') constituting the collection, or 'rise', were fitted with Origin 4.1™ for 120 s, yielding $\tau_{e1} \cong 3$ and $\tau_{e2} \cong 45$ s. Data for the relaxation, or 'fall', were fitted to a single exponential $\tau_{e3} \cong 2$ s. The double and single exponential fits have been superposed on the data points as shown (— — —). Many collections resembled the 'well rounded' form of $F_A(t)$, where it was clear the collection was substantially at steady state (zero time rate of fluorescence change) at 120 s and exhibited short rise times. An example of this is $F_C(t)$ with parameters $V_0 = 2$ V and $f = 2$ MHz, where $\tau_{e1} \cong 2$ and $\tau_{e2} \cong 9$ s. Other collections, however, deviated from this form and continued to approach steady state at 120 s, for example, $F_B(t)$ with $V_0 = 2$ V and $f = 0.5$ MHz, where

$\tau_{e1} \cong 5$ and $\tau_{e2} \cong 170$ s. The relaxation fall times for $F_B(t)$ and $F_C(t)$ were $\tau_{e3} \cong 1$ s and $\tau_{e3} \cong 2$ s, respectively[2].

Figure 7 highlights a number of key characteristics typical of DEP collections and relaxations and these are discussed further in the next section. The most important observation is that the magnitude of the fluorescence profile, or increase in fluorescence after the DEP force is switched on, $\Delta F(t)$, and the initial rate of change of fluorescence, $\dot{F}(0)$, are key measures of the DEP strength. Profiles $F_A(t)$, $F_B(t)$ and $F_C(t)$ in figure 7 show a respective decreasing DEP strength and it is clear $\Delta F_A(t) > \Delta F_B(t) > \Delta F_C(t)$ and $\dot{F}_A(0) > \dot{F}_B(0) > \dot{F}_C(0)$, that is, both $\Delta F(t)$ and $\dot{F}(0)$ concurrently follow the same trends.

4.2. Quantitative measurements

Profiles for the time-dependent normalized fluorescence $F(t)$ were evaluated as described for the above example. The number of sample points for each $(w/2 + d/2)$ characteristic was $n_c = 100$ and the number of electrode pairs was $n_{pr} = 8$. The image processing parameters all had the property $i_u - i_l = 16$, i.e. the transverse length ofthe x–y cross section designated collection area, using the expressions for the lower and upper limits in (9) with $w = d = 10$ μm, was $\Delta x = x_u - x_l \cong 1.6$ μm. Typically, the integer values ranged from $i_l = 43$ to 49 and $i_u = 59$ to 65, depending on the transverse alignment of the frames used for the set-up described in section 3.3.1. The differences in the normalized fluorescence $\Delta F(120) = F(120) - F(0)$ were calculated using (12). All collections, except for the $V_0 = 1$, $f = 2$ MHz case, were best fitted by a double exponential (15) using Origin 4.1^{TM}. The relaxation after collection was best fitted by a single exponential, with fall amplitude and time, F_3 and τ_{e3}. Values for the initial collection rates $\dot{F}(0)$ were computed using (15) with fitted amplitudes F_1 and F_2 and times τ_{e1} and τ_{e2} and values were confirmed using a linear fit to the fluorescence gradient, $\delta F/\delta t$. The particle parameters $\dot{n}_e(0)/n_e(0)$ and $\Delta n_e(120)/n_e(0)$ were evaluated using equations (13) and (16) using a nominal value of $n_e(0) = 2.8$. This enabled a comparison with theoretical predictions using an FPE model.

The values of the collection parameters, including rise and fall times τ_{e1}, τ_{e2} and τ_{e3}, are shown in table 1 (rise amplitudes F_1 and F_2 and fall amplitude F_3 are omitted for clarity).

Table 1 shows that the values of the fluorescence change at $t = 120$ s, $\Delta F(120) = F(120) - F(0)$ and $\dot{F}(0)$ concurrently follow the same trends as illustrated in figure 7 and both parameters, $\Delta n_e(120)/n_e(0)$ and $\dot{n}_e(0)/n_e(0)$, are key measures of the DEP response. The values of the particle parameters $\Delta n_e(120)/n_e(0)$ and $\dot{n}_e(0)/n_e(0)$ for set I with a constant peak voltage $V_0 = 2$ V and variable frequency $f = 0.5$, 1, 2 MHz show the DEP response decreases with increasing frequency. This is expected since equation (1) shows the DEP force is proportional to the effective polarizability of these microspheres predicted by the real part of the Clausius–Mossotti function, $\mathrm{Re}\{f_{CM}\}$, plotted in figure 9. Figure 9 shows the $\mathrm{Re}\{f_{CM}\}$ for the same low conductivity medium as used in the DEP experiments decreases 3× from 0.5 to 2 MHz and is negligible at 3 MHz—consistent with the observation of no DEP collections for $f \geqslant 3$ MHz. The values of the collection parameters $\Delta n_e(120)/n_e(0)$ and $\dot{n}_e(0)/n_e(0)$ in table 1 for set II with constant frequency $f = 2$ MHz show the DEP response markedly decreases with voltage, as predicted from the theory that predicts the DEP force $\propto V_0^2$. The rise times τ_{e1} and τ_{e2} are consistently higher than the fall time τ_{e3} for substantial DEP collections and this is expected of a system where the collection occurs under a combination of deterministic and stochastic forces, in contrast to relaxation that occurs solely by diffusion.

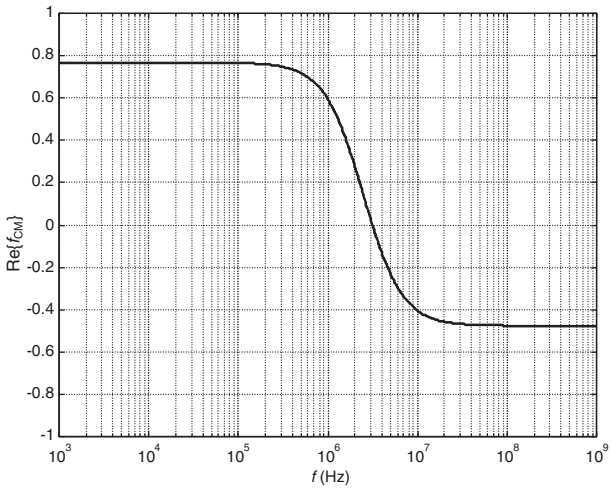

Figure 9. Frequency-dependent real part of the Clausius–Mossotti function $\mathrm{Re}\{f_{CM}\}$ used for predicting the polarizability of 216 nm diameter latex microspheres in a low conductivity medium (1.7 mS m^{-1}).

Each of the values in table 1 is an average of *three* experimental values compiled from the six sets (of three experiments) and there was statistical variation in the $F(t)$ profile between each experiment under the same V_0 and f conditions. Figure 7 indicates this statistical variation for the condition $V_0 = 2$ V by illustrating that the DEP collection profile $F_A(t)$ at $f = 1$ MHz is greater than for $F_B(t)$ at $f = 0.5$ MHz for this particular DEP experiment—-which is in contrast to the average shown in table 1. The reason for these variations between substantially strong DEP collections is not entirely clear at this stage but may be due to fluid motion (Ramos *et al* 1998, 1999, Green *et al* 2000a, 2000b) that confounds the observations and needs further investigation.

A brief comparison of the collection parameters with theoretical predictions is illustrated in figure 10. The initial collection rate $(\dot{n}_e(0)/n_e(0))$ was normalized with respect to the value at $f = 1$ MHz and $V_0 = 2$ V (an average of the two, approximately equal, values listed in each set was taken). The predicted parameter was obtained from equation (3) using the Clausius–Mossotti function which is plotted in figure 9. Figure 10 shows this parameter for different frequencies and voltages, using the data presented in table 1. Also shown is a linear regression to the data, which has a slope of unity and indicates that measurement of the ratios of the initial collection rate is an excellent indicator of the dielectrophoretic properties of the system. In contrast, the ratios of the initial to steady-state transition $(\Delta n_e(120)/n_e(0))$ are inconsistent with theoretical predictions (data not plotted). The reasons for the discrepancy between theory and experiment for the steady-state data are not

[2] The curve fitted for the relaxation $F_C(t)$ has been removed for clarity.

Table 1. Experimental frequency and voltage-dependent DEP particle collection and relaxation data. The values are an average of three separate experiments which have been rounded to two significant figures.

	Collection						Relaxation		
Set	V_0 (V)	f (MHz)	$\Delta F(120)$ ($\times 10^{-2}$)	$\dot{F}(0)$ ($\times 10^{-2}$)	$\frac{\Delta n_e(120)}{n_e(0)}$	$\frac{\dot{n}_e(0)}{n_e(0)}$	τ_{e1} (s)	τ_{e2} (s)	τ_{e3} (s)
I	2	0.5	20	3.1	58	9.4	4.1	220	1.2
	2	1	17	2.9	48	8.9	2.9	35	1.6
	2	2	10	1.5	29	4.6	2.9	17	1.4
II	4	2	21	5.9	62	18	2.3	17	1.4
	2	2	11	1.3	32	4.1	5.8	88	1.5
	1	2	1.5	0.51	4.2	1.6	3.5	—	2.5

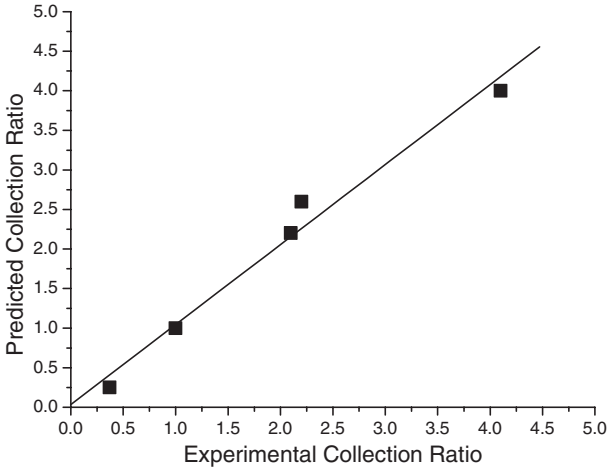

Figure 10. Correlation between experimental and predicted values of the initial collection rate. The ratios of the parameter were normalized with respect to their values at $f = 2$ MHz and $V_0 = 2$ V.

entirely clear and may be related to limitations in the model or to experimental effects such as mentioned above.

5. Conclusion

Video recorded fluorescence microscopy was used to measure and quantify the time-dependent dielectrophoretic collections of 216 nm diameter carboxyl-modified latex microspheres onto 10 μm width 10 μm gap planar interdigitated electrodes as a function of frequency and applied voltage. Analytical methods utilizing the geometrical properties of the electrode array and implemented in MATLAB 5.0™ were used to characterize the dielectrophoretic response of the microspheres. The time-dependent particle collections, in the near vicinity of each electrode edge, were characterized by three parameters: the initial DEP collection rate, the transition from initial to pseudo-steady-state at 120 s and the rise time. The relaxation profiles were summarized by the fall time parameter.

Collection time profiles exhibited a clear decrease in the DEP response as the frequency increased from 500 kHz to 2 MHz and this trend concurred with the reduction in the real part of the effective polarizability of the microspheres predicted by the Clausius–Mossotti function. The DEP response also decreased as the peak electrical potential was reduced from 4 to 1 V and the trend concurred with a square-law voltage dependence of the DEP force. The trends in the rise times are not as conclusive. However, the results show rise times are greater than the fall times for appreciable DEP collections, as expected from system dynamics. The initial DEP collection rate parameter was in good agreement with the predicted variation in DEP force at different applied voltages and frequencies, as given by equation (3). However, the initial to pseudo-steady-state transition was not as sensitive as theory predicts. Both parameters are dependent on particle concentration but in practice this technique is only suitable for a limited range of concentrations. At low concentrations there are insufficient particles collecting during a reasonable time frame to yield useful data; at high concentrations particle interactions and background fluorescence complicate the analysis. The analytical methods described in this paper show a promising application for characterizing the dielectrophoretic collections of sub-micron particles using fluorescence microscopy.

References

Abramowitz S 1996 Towards inexpensive DNA diagnostics *Trends Biotechnol.* **14** 397–401

Asbury C L 1999 Manipulation of DNA using nonuniform oscillating electric fields *PhD Dissertation* University of Washington, Seattle, USA

Asbury C L and van den Engh G 1998 Trapping of DNA in nonuniform oscillating electric fields *Biophys. J.* **74** 1024–30

Asbury C L, Diercks A H and van den Engh G 2002 Trapping of DNA by dielectrophoresis *Electrophoresis* **23** 2658–66

Bakewell D J 2002 Dielectrophoresis of colloids and polyelectrolytes *PhD Dissertation* University of Glasgow, Scotland, UK

Bakewell D J and Morgan H 2001 Measuring the frequency dependent polarisability of colloidal particles from dielectrophoretic collection data *IEEE Trans. Dielectr. Electr. Insul.* **8** 566–71

Bangs 1997 *Technical Notes #49 and #206* Bangs Laboratories Inc., USA

Cheng J, Sheldon E L, Wu L, Uribe A, Gerrue L O, Carrino J, Heller M J and O'Connell J P 1998 Preparation and hybridisation analysis of DNA/RNA from *E.Coli* on microfabricated bioelectronic chips *Nature Biotech.* **16** 541–6

Chou C-F, Tegenfeldt J O, Bakajin O, Chan S S, Cox E C, Darnton N, Duke T and Austin R H 2002 Electrodeless dielectrophoresis of single- and double-stranded DNA *Biophys. J.* **83** 2170–9

Crippen S M, Holl M R and Meldrum D R 2000 Examination of dielectrophoretic behaviour of DNA as a function of frequency from 30 Hz to 1 MHz using a flexible microfluidic test apparatus *Proc. Micro Total Analysis Systems* ed A van den Berg *et al* (Dordrecht: Kluwer) pp 529–32

Cui L, Holmes D and Morgan H 2001 The dielectrophoretic levitation and separation of latex beads in microchips *Electrophoresis* **22** 3893–901

Gardiner C W 1985 *Handbook of Stochastic Methods for Physics, Chemistry, and the Natural Sciences* (Berlin: Springer)

Gascoyne P R C, Noshari J, Becker F F and Pethig R 1994 Use of dielectrophoretic collection spectra for characterizing differences between normal and cancerous cells *IEEE Trans. Ind. Appl.* **30** 829–33

Green N G, Ramos A, Gonzalez A, Morgan H and Castellanos A 2000a Fluid flow induced by non-uniform AC electric fields in electrolytic solutions on micro-electrodes. Part I: experimental measurements *Phys. Rev.* E **61** 4011–8

Green N G, Ramos A and Morgan H 2000b AC electrokinetics: a survey of sub-micrometre particle dynamics *J. Phys. D: Appl. Phys.* **33** 632–41

Haskell B G, Puri A and Netravali A N 1997 *Digital Video: An Introduction to MPEG-2* (Boston: Kluwer)

Jones T B 1995 *Electromechanics of Particles* (Cambridge: Cambridge University Press)

Milner K R, Brown A P, Betts W B, Goodall D M and Allsopp D W E 1998 Analysis of biological particles using dielectrophoresis and impedance measurement *Biomed. Sci. Instrum.* **34** 157–62

Morgan H and Green N 2003 *AC Electrokinetics: Colloids and Nanoparticles* (Baldock, Herts: Research Studies Press)

Morgan H, Izquierdoa G, Bakewell D, Green N G and Ramos A 2001 The dielectrophoretic and travelling wave forces for interdigitated electrode arrays: analytical solution using Fourier series *J. Phys. D: Appl. Phys.* **34** 1553–561

Pacansky J and Lyerla J R 1979 Photochemical decomposition mechanisms for AZ-type photoresists *IBM Res. Dev.* **23** 42–55

Ploem J S and Tanke H J 1987 *Introduction to Fluorescence Microscopy* (Oxford: Oxford University Press)

Pohl H A 1978 *Dielectrophoresis* (Cambridge: Cambridge University Press)

Ramos A, Morgan H, Green N G and Castellanos A 1998 AC electrokinetics: a review of forces in microelectrode structures *J. Phys. D: Appl. Phys.* **31** 2338–53

Ramos A, Morgan H, Green N G and Castellanos A 1999 AC electric-field-induced fluid flow in microelectrodes *J. Colloid Interface Sci.* **217** 420–2

Suehiro J, Yatsunami R, Hamada R and Hara M 1999 Quantitative estimation of biological cell concentration suspended in aqueous medium by using dielectrophoretic impedance measurement method *J. Phys. D: Appl. Phys.* **32** 2814–20

Talary M S and Pethig R 1994 Optical technique for measuring the positive and negative dielectrophoretic behaviour of cells and colloidal suspensions *IEE Proc. Sci. Meas. Technol.* **141** 395–9